HHS Public Access

Author manuscript

Nat Struct Mol Biol. Author manuscript; available in PMC 2012 November 02.

Published in final edited form as:

Nat Struct Mol Biol. 2010 May ; 17(5): 590–595. doi:10.1038/nsmb.1820.

Direct observation of the myosin-V power stroke and its reversal

James R. Sellers[1] and **Claudia Veigel**[2,3]

[1]Laboratory of Molecular Physiology, National Heart, Lung and Blood Institute, NIH, Bethesda, MD USA 20892

[2]Physical Biochemistry, National Institute for Medical Research, The Ridgeway, Mill Hill, London NW7 1AA, UK

[3]Department of Cellular Physiology, Ludwig Maximilians Universität München, Schillerstrasse 44, 80336 München, Germany

Abstract

Complex forms of cellular motility, including cell division, organelle trafficking or signal amplification in the auditory system, require strong coordination of the myosin motors involved. The most basic mechanism of coordination is via direct mechanical interactions of individual motor heads leading to modification of their mechano-chemical cycles. Here we used an optical trap-based assay to investigate the reversibility of the force- generating conformational change (power stroke) of single myosin-V motor heads. By applying load to the head shortly after binding to actin, we found that at a certain load the power stroke could be reversed and the head fluctuated between an actin-bound pre- and a post-power stroke conformation. This load-dependent mechanical instability might be critical to coordinate the heads of processive, dimeric myosin-V. Non-linear response to load leading to coordination or oscillations amongst motors might be relevant for many cellular functions.

Class Va myosins are ATP driven two-headed motor proteins expressed in neurons and melanocytes that transport neuronal vesicles and melanosomes along actin [1]. The motor moves its cargo processively, taking tens of 36 nm steps per interaction event [2–5]. Each myosin head consists of an N-terminal catalytic domain that hydrolyses ATP and binds to actin. This is followed by the neck domain, an extended α-helix, stabilised by binding light chains of the calmodulin family, that serves as a lever arm. The neck extends into a coiled-coil dimerisation and cargo-binding domain. It is generally thought that during each biochemical cycle a single myosin-V motor head binds to actin with hydrolysis products phosphate and ADP bound. According to the power-stroke model, actin binding induces phosphate release and a force-generating conformational change of the bound head. This

Correspondence should be addressed to: Claudia Veigel, Department of Cellular Physiology, Ludwig-Maximilians-Universität München, Schillerstrasse 44, 80336 München, Germany, claudia.veigel@med.uni-muenchen.de.

Author contributions: J.R.S. expressed and purified MVS1; C.V. carried out experiments and data analysis and J.R.S. and C.V. wrote the paper.

Competing financial interests: The authors declare that they have no competing financial interests.

leads into an ADP-bound state. When ADP is released, a second, smaller conformational change takes place before the head finally binds a new ATP, detaches from actin and hydrolyses the ATP [3,4,6–8]. Evidence for an actin-bound pre-power stroke state, preceding the main conformational change, comes from crystal structures of myosin alone [9] and electron micrographs of myosin-V bound with both heads to actin [10,11]. In the latter studies backward and forward leaning orientations of the base of the lever arm could be distinguished, that are thought to correspond to pre- and post-power stroke conformations. The model motivated by these data postulates that each processive step of dimeric myosin-V along actin causes the neck domains of the two bound heads to switch orientation in a reciprocal manner: the lead head from backward to forward and the trailing head from forward to backward leaning orientation. These orientations have then been studied by attaching fluorescent labels to the neck domains [12,13]. In a number of pioneering experiments, translational [14–16] and rotational motion of the neck (using microtubule fragments as markers of angular motion) [17] during transitions between successive, actin-bound orientations were also resolved. However, the reversibility of the transition from pre- to post-power stroke state has never been directly observed. It has been shown that dimeric myosin-Va stalls at a load of ~2 pN [2,4,16,18] and slides backwards at higher forces [19], similar to kinesin-1(ref [20]). It had remained unclear, however, whether these backward movements involve power stroke reversal or whether the molecule simply unbinds and rebinds. An interesting regulatory mechanism would emerge if the power stroke could be reversed while the motor stays attached to actin. This would cause a sudden release of tension under load, i.e. a negative compliance, without cargo detachment. We therefore set out to test the reversibility of the power stroke of a single myosin motor head, using single molecule mechanical experiments.

RESULTS

Detection of power stroke reversals

In order to investigate whether the force generating conformational change of a single myosin head is reversible and whether we could resolve transitions between pre- and post-power stroke conformations, we designed an optical-trap based single-molecule experiment with which we could rapidly detect myosin binding and subsequently apply constant backward load. We used a three-bead assay where recombinant, single-headed myosin-V constructs containing 6 IQ motifs (MVS1) [21] were immobilised on surface-attached beads and allowed to interact with an actin filament suspended between two beads, held in optical traps [22,23] (Fig. 1a). We used a high ATP concentration (100 μM) to be close to physiological conditions and the nucleotide-free rigor state was short-lived (see below). Force acting on the actin filament was determined by the displacement Δx of the trapped beads from the centres of the traps. In order to increase time resolution in detecting myosin binding, bead 1 was rapidly oscillated (1 kHz) with a small amplitude while the position of bead 2 was monitored, as in earlier studies [21]. The time point of myosin binding was detected on-line by analysing change in amplitude of the sinusoidal forcing function transmitted from bead 1 to bead 2 (see Methods) and setting a threshold. Thermal noise caused false alarms in the detection of binding and detachment. By appropriately setting the threshold for detecting binding, we could shift the false alarms either to the unbound or

bound state. We chose the former. To probe for power-stroke reversal, we applied backward loads varying between 2 and 7 pN by displacing both traps rapidly by a fixed distance immediately after detecting binding (Methods, Supplementary Fig. S1a). The threshold for detecting binding was tuned such that the position of both traps was stationary during myosin attachment events while spurious trap displacements were tolerated during the unbound periods (Fig. 1b). We could thus follow conformational changes of the bound motor under near-constant loads with ~1 ms time resolution. As soon as myosin detachment was detected, the traps were returned to their initial positions, so that the sequence could be repeated. The power stroke following initial binding was not resolved within our time resolution of ~ 1 ms and it is likely that at low load, myosin binding was only detected after the motor had reached the post-power stroke state [23,24]. During attachment, intermittent back and forth displacements were observed (Fig. 1b, blue arrows), consistent with a reversal of the initial conformational change.

Detailed inspection of a typical binding event (Fig. 1c) allows us to assign time points of transitions (cartoon Fig. 1d). Myosin binding and (the unresolved first) power stroke happened around time point t_1. With ~3 ms delay both traps were displaced at t_2, so that a backward load of ~ 3 pN was applied. Note that the displacement occurring between t_1 and t_2 is due to the movement of the traps and not a power stroke. Variables and geometry are defined in Fig. 1d. At t_3, a negative displacement ('reversal') of ~20 nm occurred, followed by a positive displacement ('recovery') of similar amplitude at t_4 (Fig. 1c). This shows that the bound motor could reverse into the pre-power stroke conformation (pre-state), but subsequently also recover its post-power stroke conformation (post-state).

Load dependent amplitudes of reversals and recoveries

Next we analysed the amplitudes of the reversals and recoveries in order to test whether they correspond to complete power strokes. We used a running t-test to detect transitions between distinct bound positions (Fig. 1c, Methods) and found transitions in ~20 – 30% of binding events at forces between 2–7 pN, while below 1.5 pN transitions were not observed (Fig. 2a and Supplementary Fig. S1c). Up to 7 back-and-forth transitions per binding event were found at forces between 2 and 3 pN, while above 5 pN transitions were overwhelmingly backwards (Fig. 2d). The average number of transitions per binding event over the entire force range (2–7 pN) was ~1.6 (Supplementary Fig. S1d). The majority (60–70%) of final transitions before detachment were reversals at all forces (Fig. 1b and Supplementary Fig. S3c). This suggests that the motor in pre-power stroke conformation is less strongly bound [6,7,19]. To be less sensitive to slow baseline drift, amplitudes of both reversals and recoveries were measured as relative displacements in Fig. 2a (relative to the position preceding the respective transition). Fig. 2b shows the distribution of reversals and recoveries detected over the entire range of forces. This distribution could be fitted by sums of Gaussians. For reversals, we identified a main (16 ± 9 nm), and two minor contributions (35 ± 3 nm and 46 ± 7 nm, mean ± SD), for recoveries a single contribution (12 ± 7nm). Average amplitudes of all three populations of reversals were independent of load (Fig. 2c,d). Comparing amplitudes, it is likely that the main reversals are the direct inversions of the recoveries. We attribute the large backward displacements (> 25 nm) to slippage along actin (i.e. fast detachment and reattachment) because their relative frequency increased with

increasing load (Fig. 2c, d). Slippage along the helical repeat of the actin filament could explain the population of ~ 35 nm backward displacements, while a combination of slippage and power stroke reversal could cause displacements with ~ 46 nm amplitude. This interpretation is supported by the fact that some large backward displacements were followed by a recovery stroke (16 ± 5 nm, Supplementary Fig. S3d), although many were followed by detachment.

To be able to directly compare reversals to power strokes in the same experimental conditions we measured the power stroke produced in absence of applied load (< 2 pN) with a different method. Applying our standard ensemble-averaging technique [21,25] we aligned and averaged myosin binding events using the time points of binding to or detachment from actin respectively (Fig. 2c). As seen before, an initial power stroke (~15 nm) was produced within 1 ms after binding to actin, while a much smaller second displacement (~5 nm) followed with some delay of ~29 ms. This is roughly consistent with the reported ADP release rate [4,6,7,26] taking differences in temperature into account (here k_1 = 24 s^{-1}, T = 29°C). These experiments were carried out at low ATP (10 μM) so that we could clearly resolve the second displacement and the subsequent, ATP-dependent dwell time (~30 ms) [4,8,21,25]. The ATP-binding rate was ~2.4$\mu M^{-1}s^{-1}$, consistent with previous data [6,7,26]. We therefore expect that in the load experiments, carried out at 100 μM ATP, the motor will spend most of the actin-bound dwell time in an ADP-bound state because the nucleotide-free rigor state following ADP-release will be comparatively short-lived (i.e. ~3 ms for ATP-binding and detachment, assuming the above ATP binding rate). Thus, when comparing the reversals at high ATP and high load to the power strokes at low ATP and low load we need to compare to the initial 15 nm, not the whole 20 nm power stroke. With these constraints the numbers support the conclusion that the observed transitions at high load reflect complete reversals and recoveries of the main myosin power stroke component.

Load dependent kinetics of power stroke reversals and recoveries

Next we evaluated how load affects the kinetics of the observed transitions. Since the transition from pre- to post-power stroke state is the main force generating transition, we expected the dwell times of both pre- and post-power stroke states to be strongly, but oppositely affected by load. We therefore analysed the load dependence of dwell times in the two states (Fig. 3, 100 μM ATP). Cumulative distribution plots of dwell times in the pre-state (Fig. 3a) were well described by a single exponential function (Methods, eq. 1), while two exponential components were required to fit the dwell time distributions in the post-state (Fig. 3b, Methods, eq. 2). This suggests two distinct post-power stroke states, a short-lived and a long lived component $post_1$ and $post_2$ (Supplementary Fig. S2). To keep the scheme (Fig. 3d) simple at first, we lumped the two post-power stroke states into one and calculated a single rate constant for reversal at different loads (Method, eq. 3). Here we define the reversal rate as the reciprocal of the average dwell time in post-state, while the recovery rate is the reciprocal of the one in pre-state (Methods). The ratio of the two rates gives the probability to find the motor in either a pre- or a post-power stroke conformation at different loads while bound to actin. The reversal rate increased with increasing load, while the opposite was observed for the recovery rate (Fig. 3c), consistent with an Arrhenius-type

transition between pre- and post-power stroke conformations (eq. 4). Equal probability to find the motor in pre- or post-power stroke conformation was reached at ~4 pN.

Biochemical state of power stroke reversals and recoveries

Having collected the evidence for power-stroke reversal still leaves open the question to what degree the biochemical pathway is followed backwards. Several lines of evidence suggest that acto-myosin-V has ADP bound at the catalytic site when it is held in a bi-stable state between pre-and post-power stroke conformation. Given an off-rate of > 250 s^{-1} in solution [6], phosphate was probably mostly released by the time load was applied (after ~3 ms). The concentration of phosphate in solution was low (< 2 μM) and made phosphate rebinding unlikely. To investigate whether phosphate could rebind to the acto-myosin-V complex under load we did a control experiment (Fig. 4b) which shows that at forces > 2 pN, addition of 10 mM phosphate increases the rate constant for unbinding by a factor of two. This suggests that phosphate may rebind and that the phosphate-bound pre-power stroke conformation (A.M.ADP.Pi) detaches more easily. This is consistent with previous reports that this state is bound more weakly [27,28]. The effect of phosphate could also be non specific, but this appears unlikely because the effect is not observed in the absence of load (Fig. 4b). This is consistent with a partial reversal of the chemical cycle coupled to the reversal of the mechanical cycle. It further follows that most motors must have had their phosphate released before load was applied in our experiments when phosphate was not added. Finally, it was also unlikely that the motor dwelled in a nucleotide free rigor state as argued above, because we intentionally worked at high ATP concentration (100 μM). Thus, all the evidence suggests that the myosin motor in the ‘rocking crossbridge’ state has released phosphate and retains ADP.

DISCUSSION

In summary, our experiments have provided a new view on the mechano-chemical energy landscape guiding myosin force generation (Fig. 4a). Two lines of evidence suggest that at high loads the myosin-V motor can switch back and forth between post- and pre-power stroke conformations while remaining bound to actin. First, amplitudes of reversals and recoveries were similar, independent of load and matched the main component [11,29,30] of the two-step power stroke[4,8,21] at low load. Second, the dwell times of reversals became longer, while those of recoveries became shorter at increasing load, as expected. This finding is direct evidence for the ‘rocking crossbridge’, hypothesised by Huxley and Simmons in 1971[ref31], but never observed at the level of a single molecule.

The effect of load on a single myosin-V motor head can be divided into three force regimes, as shown in Figs 3c and 4a. At low forces F_I (0 – 2 pN) the actin-bound dwell time increases with load. At intermediate forces F_{II} (2 – 5 pN) the motor switches back and forth between pre and post-power stroke conformations, while at high forces F_{III} (5 – 7 pN) the motor dwells predominantly in the pre-power stroke conformation before being forced to detach.

At low forces F_I, actin-bound dwell times increased about two-fold with load. This is consistent with a load dependent and rate limiting ADP release [2,4,6,7,18,21,30,32]. ATP binding, in contrast, was shown to be weakly load dependent [21,30,33] and the rigor state is

negligible at high ATP (100 μM) as discussed. ADP-release is probably slowed down because the second step of the working stroke, associated with ADP release, is hindered [8,21]. The sensitivity of a biochemical transition to load is typically expressed as a distance *d* to the transition state [34]. We find here *d* = 2.1 nm (at 29°C, Fig. 3c) which is roughly consistent with, though slightly smaller than, what we found previously (*d* = 4.3 nm at 23 °C, ref[21]). This difference might be due to differences in temperature [26]. Uemura *et al.* [16] reported an even larger distance of 12.5 nm for ADP-release. However these results can perhaps be reconciled. A strong sensitivity to force is exactly what one expects approaching a non-linearity in response, such as power stroke reversal. Uemura *et al*[16] observed a softening in response (i.e. increased sensitivity to load) in the range of 1.5 – 2 pN which is precisely where we begin to see power stroke reversals. Also at this force the Rief-group has observed processive backward stepping of the dimeric motor [27,35].

While backward load only weakly affects total duration of myosin binding at intermediate force F_{II} (2 – 5 pN), it shifts the motor increasingly into a pre-power stroke ADP-bound state. Our 'stall force' (~ 4 pN) for a single head, i.e. equal probability to dwell in pre and post-power stroke conformation, is somewhat higher than the external force required to stall processive movement of the myosin-V dimer (1.7 – 3 pN) [2,4,16,18,19,27]. The difference is likely to be due to differences in geometry of force application. For the full length dimer the effective lever arm is likely to be longer than in our single headed construct which can qualitatively explain the difference.

What is the relevance of the power stroke reversibility for the mechanical head-head communication during processive forward movement of a myosin-V dimer? Due to differences in geometry it is again difficult to directly compare absolute forces. However it is conceivable that the force exerted by the trailing head on the lead head is enough to keep the leading head in pre-power stroke conformation until the trailing head detaches, as suggested by electron and fluorescence microscopy [10–12,36] and solution kinetic studies [3,7,37,38] (Supplementary Fig. S5(i and ii)). This scenario is also consistent with our previous observation [4,21] of an only two-fold acceleration of ADP-release on the trailing head in the dimer compared to a single head. The twofold acceleration would correspond to a force of ~1.5–2 pN [4,21,39], less than what would be expected if the lead head was in post-power stroke state (~3.5 pN) [21,39].

We also found rare binding events with very slow detachment kinetics in this force range F_{II} (Supplementary Table 1), similar to what was described for processive backward stepping of myosin-V at super stall forces [19]. Since only the reversals (post-power stroke state) but not the recoveries (pre-power stroke state) show a slow component, the motor spending time in post-power stroke state 2, $post_2$, must be responsible (Supplementary Fig. S2). At present the exact nature of the short and long-lived post-power stroke states is not clear. During processive forward movement at low load both ADP-bound states might occur in sequence (Fig. 4a, A.M.ADP and Supplementary Fig. S2a) with the shorter lived state first ($post_1$), followed by an isomerisation to a more stable post-power stroke state ($post_2$) [7,38,40].

At high forces F_{III} (5–7 pN) we found that the motor was forced to detach, predominantly from pre-power stroke conformation. This is consistent with previously measured unbinding forces for a single myosin-V head [32,41].

If we want to determine efficiency of a single motor head at increasing load we simply need to know whether the head detaches from pre- or post-power stroke conformation. Efficiency can be defined as the total work done against external load up to a time point immediately before detachment, divided by the free energy gained by hydrolysis of one ATP molecule. In regime F_I (<2 pN, Fig. 4c) we do not observe reversals and therefore the motor always detaches from post-power stroke state. The efficiency E is $E = Fd_{stroke}/\Delta G_{ATP}$. In regime F_{II} (2–5 pN) the motor detaches in approximately 30% of binding events from post-power stroke conformation (Supplementary Fig. S3c). Here $E = F$ 0.3 $d_{stroke}/\Delta G_{ATP}$, while in force regime F_{III} the motor detaches predominantly from the per-power stroke state and does not produce work. What does this signify for the efficiency of the dimer? Maximum work output can be expected close to stall force, but the precise value of the efficiency will depend on the exact geometries of forces and motion.

Complex load sensitivity at different stages of the chemo-mechanical cycle as observed here has obvious implications for the collective dynamics of myosin motors. Load dependent ADP release might contribute to coordinating the two heads of processive dimeric myosin-Va [3,4,7,19,21,32]. Reversibility of the power stroke at higher loads provides, on the one hand, a microscopic mechanism for backward sliding at super stall forces [19]. On the other hand, reversibility of the power stroke is equivalent to a highly non-linear response which can lead to mechanical synchronisations and oscillations. Power stroke reversals could thus be involved in the wide range of such phenomena, for example in certain types of muscle [42,43], or in mechano-receptive hair bundles in the sensory cells of the inner ear [44,45].

METHODS

Protein preparations, solutions and optical trapping conditions

We used a baculo-virus expressed mouse myosin-Va fragment S1 (MVS1) as described previously [21]. Details on the myosin construct, biochemical solutions and on optical trapping conditions are described in the Supplementary Information online. Procedures to apply load and details on data analysis are given below and also in the Supplementary Information online.

Application of load

To improve time resolution for detecting myosin binding we oscillated the position of one optical trap at a frequency f = 1 kHz and amplitude A_0 = 35 nm parallel to the actin filament axis using a sinusoidal function [25,33]. Because of low trap stiffness and viscous damping this caused the position of the bead - actin - bead dumb-bell held in the traps to oscillate parallel to the filament axis with r.m.s. amplitude of only ~7 nm during the intervals when no myosin was bound to actin. During periods when myosin was bound this r.m.s. amplitude was further reduced to less than 1.5 nm so that the mechanical disturbance of the bound myosin was very small (corner frequency of thermal noise during attachment ~ 3 kHz; r.m.s.

of 1 kHz signal close to thermal background noise). By analysing changes in variance of the high pass filtered displacement signal (dominated by the 1 kHz signal during periods when myosin was not bound) transmitted to the bead in the other (passive) trap we could detect myosin binding with ≈1 ms time resolution [21]. Changes in this signal were used to produce a trigger signal. The latter was used to change the position of both optical traps [33]. To apply load, both traps were moved by a distance dx_{trap} in parallel to the actin filament axis to produce a force, $F = 2\kappa_{trap}\Delta x$ (with κ_{trap}: single trap stiffness; $\Delta x = x_{trap} - x_{bead}$; x_{trap}: trap position; x_{bead}: bead position) [23]. Here we assume the stiffness of both traps to be the same. Following detection of myosin detachment, the traps were returned to their rest position, again with a time delay of ≈ 3 ms. Initial binding and conformational change occurred within less than our time resolution, so that the direction of the initial conformational change was not resolved in individual binding events. We therefore determined its direction for each actin dumb-bell by analysing an ensemble of myosin binding events in absence of load [24], before load experiments were performed.

Analysis of amplitudes of reversals and recoveries

Data analysis was carried out on the displacement data recorded from the bead held in the passive trap. Amplitudes and dwell times of reversals and recoveries were analysed off-line in an automated fashion. The *t*-test values were calculated from the time series of variance and mean displacement over a running time window of 20 data points. To determine the amplitudes of reversals and recoveries we calculated the time averaged displacement between level changes. Amplitudes were calculated relative to the preceding level.

When load was applied by moving both traps in a stepwise fashion, the actin dumbbell, connected to the surface via myosin, first produced a passive, series elastic response (Supplementary Fig. S1a). To separate the elastic response from subsequent power stroke reversals we determined the bead position 2 ms after load was applied and the system had relaxed [46]. This bead position was used as reference for subsequent reversals.

Analysis of dwell times

The minimum dwell time t_{min} of a myosin binding event, we evaluated, was t_{min} = 10 ms. t_{min} of pre and post-states evaluated during a binding event was t_{min} = 4 ms and the maximum dwell time t_{max} = 500 ms. Dwell-time distributions of pre-states and post-states were plotted as cumulative and normalised distributions. Rate constants *k* were obtained by least squares fitting of the model functions. Fig. 3d shows the reaction scheme used to describe transitions between pre and post-state and detachment (D). Cumulative dwell-time distributions were described by a probability density function, taking the limits t_{min} and t_{max} into account [19,47]. If a single exponential could be used to describe the distribution, the function was

$$P_b(t)=\frac{\exp(-kt)-\exp(-kt_{\min})}{\exp(-kt_{\max})-\exp(-kt_{\min})} \quad (1)$$

The exit rate out of a state *k* is equal to the reciprocal of the average dwell time of that state. If two exponential components were required to fit the dwell time distributions, the probability density function was

$$P_b(t)=\frac{Z_1(\exp(-k_1t)-\exp(k_1t_{\min}))+(1-Z_1)(\exp(-k_2t)-\exp(-k_2t_{\min}))}{Z_1(\exp(-k_1t_{\max})-\exp(k_1t_{\min}))+(1-Z_1)(\exp(-k_2t_{\max})-\exp(-k_2t_{\min}))} \quad (2)$$

Z_1 and (1-Z_1) are the relative amplitudes of the fast and slow component respectively.

If binding events ended on a reversal, these last reversals preceding detachment were not taken into account in the kinetic analysis because they could be due to reversal of the power stroke or slippage along actin. If slippage had occurred, the state would be ambiguous, i.e. either pre or post-power stroke conformation (see Supplementary information). The exit rate *k* out of the pre-state in our analysis thus characterises the transition into post-state and is called recovery rate. The state before the first reversal in a binding event has to be a post-power stroke state. Therefore, we included these dwell times into the population of post-states. At all loads most of the binding events ended on a backward displacement (Supplementary Fig. S3c). The exit rate *k* out of the post-state in our analysis therefore mostly characterises transition into pre-state and is called reversal rate.

The average reversal rate *k* at different loads was calculated from the two reversal rates k_1 and k_2 obtained from the dwell time distibutions of the post-state (Fig. 3b):

$$k=0.5(Z_1k_1+(1-Z_1)k_2) \quad (3)$$

Load dependence of the average and the two individual reversal rates k_1 and k_2 was described by an Arrhenius-type transition over an activation energy barrier,

$$k(F)=k_0\exp(-\frac{Fd}{k_bT}) \quad (4)$$

k(F): load dependent rate, k_0: rate in absence of load, *F*: force, *d*: distance parameter, k_bT: thermal energy.

For the recovery rate and for the detachment rate of motors, two exponential components were required to describe their load dependence.

$$k(F)=k_{01}\exp(-\frac{Fd_1}{k_bT})+k_{02}\exp(-\frac{Fd_2}{k_bT}) \quad (5)$$

Preparation of Figures

Figures were generated using standard software Windows Excel and CorelDraw.

Supplementary Material

Refer to Web version on PubMed Central for supplementary material.

Acknowledgments

We thank Christoph Schmidt, III. Physikalisches Institut, Universität Göttingen, Germany and Justin Molloy, National Institute for Medical Research, London, UK for stimulating discussions. We also thank Estelle Harvey, Laboratory of Molecular Physiology, NHLBI, NIH Bethesda, USA for technical assistance and John Hammer III, Laboratories of Cell Biology, NHLBI, NIH Bethesda, USA for kindly supplying the myosin-V clone. We are also grateful to the MRC, The Royal Society and NIH for grant support.

References

1. Sellers JR, Veigel C. Walking with myosin V. Curr Opin Cell Biol. 2006; 18:68–73. [PubMed: 16378722]
2. Mehta AD, et al. Myosin-V is a processive actin-based motor. Nature. 1999; 400:590–593. [PubMed: 10448864]
3. Sakamoto T, Webb MR, Forgacs E, White HD, Sellers JR. Direct observation of the mechanochemical coupling in myosin Va during processive movement. Nature. 2008; 455:128–U99. [PubMed: 18668042]
4. Veigel C, Wang F, Bartoo ML, Sellers JR, Molloy JE. The gated gait of the processive molecular motor, myosin V. Nat Cell Biol. 2002; 4:59–65. [PubMed: 11740494]
5. Yildiz A, et al. Myosin V walks hand-over-hand: Single fluorophore imaging with 1.5-nm localization. Science. 2003; 300:2061–2065. [PubMed: 12791999]
6. De La Cruz EM, Wells AL, Rosenfeld SS, Ostap EM, Sweeney HL. The kinetic mechanism of myosin V. Proc Natl Acad Sci USA. 1999; 96:13726–13731. [PubMed: 10570140]
7. Rosenfeld SS, Sweeney HL. A model of myosin V processivity. J Biol Chem. 2004; 279:40100–40111. [PubMed: 15254035]
8. Volkmann N, et al. The structural basis of myosin v processive movement as revealed by electron cryomicroscopy. Mol Cell. 2005; 19:595–605. [PubMed: 16137617]
9. Coureux PD, Sweeney HL, Houdusse A. Three myosin V structures delineate essential features of chemo-mechanical transduction. EMBO J. 2004; 23:4527–4537. [PubMed: 15510214]
10. Walker ML, et al. Two-headed binding of a processive myosin to F-actin. Nature. 2000; 405:804. [PubMed: 10866203]
11. Burgess S, et al. The prepower stroke conformation of myosin V. J Cell Biol. 2002; 159:983–991. [PubMed: 12499355]
12. Forkey JN, Quinlan ME, Shaw MA, Corrie JET, Goldman YE. Three-dimensional structural dynamics of myosin V by single-molecule fluorescence polarization. Nature. 2003; 422:399–404. [PubMed: 12660775]
13. Toprak E, et al. Defocused orientation and position imaging (DOPI) of myosin V. Proc Natl Acad Sci USA. 2006; 103:6495–6499. [PubMed: 16614073]
14. Dunn AR, Spudich JA. Dynamics of the unbound head during myosin V processive translocation. Nat Struct Mol Biol. 2007; 14:246–248. [PubMed: 17293871]
15. Cappello G, et al. Myosin V stepping mechanism. Proc Natl Acad Sci USA. 2007; 104:15328–15333. [PubMed: 17878301]
16. Uemura S, Higuchi H, Olivares AO, De La Cruz EM, Ishiwata S. Mechanochemical coupling of two substeps in a single myosin V motor. Nat Struct Mol Biol. 2004; 11:877–883. [PubMed: 15286720]
17. Shiroguchi K, Kinosita K. Myosin V walks by lever action and Brownian motion. Science. 2007; 316:1208–1212. [PubMed: 17525343]
18. Rief M, et al. Myosin-V stepping kinetics: A molecular model for processivity. Proc Natl Acad Sci USA. 2000; 97:9482–9486. [PubMed: 10944217]

19. Gebhardt JCM, Clemen AEM, Jaud J, Rief M. Myosin-V is a mechanical ratchet. Proc Natl Acad Sci USA. 2006; 103:8680–8685. [PubMed: 16731631]
20. Carter NJ, Cross RA. Mechanics of the kinesin step. Nature. 2005; 435:308–312. [PubMed: 15902249]
21. Veigel C, Schmitz S, Wang F, Sellers JR. Load-dependent kinetics of myosin-V can explain its high processivity. Nat Cell Biol. 2005; 7:861–869. [PubMed: 16100513]
22. Finer JT, Simmons RM, Spudich JA. Single myosin molecle mechanics-piconewton forces and nanometre steps. Nature. 1994; 368:113–119. [PubMed: 8139653]
23. Veigel C, Bartoo ML, White DCS, Sparrow JC, Molloy JE. The stiffness of rabbit skeletal actomyosin cross-bridges determined with an optical tweezers transducer. Biophys J. 1998; 75:1424–1438. [PubMed: 9726944]
24. Molloy JE, Burns JE, Kendrick-Jones J, Tregear RT, White DCS. Movement and force produced by a single myosin head. Nature. 1995; 378:209–212. [PubMed: 7477328]
25. Veigel C, et al. The motor protein myosin-I produces its working stroke in two steps. Nature. 1999; 398:530–533. [PubMed: 10206648]
26. Robblee JP, Cao WX, Henn A, Hannemann DE, De La Cruz EM. Thermodynamics of nucleotide binding to actomyosin V and VI: A positive heat capacity change accompanies strong ADP binding. Biochemistry. 2005; 44:10238–10249. [PubMed: 16042401]
27. Kad NM, Trybus KM, Warshaw DM. Load and Pi control flux through the branched kinetic cycle of myosin V. J Biol Chem. 2008; 283:17477–17484. [PubMed: 18441369]
28. Takagi Y, Shuman H, Goldman YE. Coupling between phosphate release and force generation in muscle actomyosin. Philos Trans R Soc Lond, Ser B: Biol Sci. 2004; 359:1913–1920. [PubMed: 15647167]
29. Moore JE, Krementsova EB, Trybus KM, Warshaw DM. Myosin V exhibits a high duty cycle and large unitary displacement. J Cell Biol. 2001; 155:625–635. [PubMed: 11706052]
30. Purcell TJ, Sweeney HL, Spudich JA. A force-dependent state controls the coordination of processive myosin V. Proc Natl Acad Sci USA. 2005; 102:13873–13878. [PubMed: 16150709]
31. Huxley AF, Simmons RM. Proposed mechanism of force generation in striated muscle. Nature. 1971; 233:533–538. [PubMed: 4939977]
32. Oguchi Y, et al. Load-dependent ADP binding to myosins V and VI: implications for subunit coordination and function. Proc Natl Acad Sci USA. 2008; 105:7714–7719. [PubMed: 18509050]
33. Veigel C, Molloy JE, Schmitz S, Kendrick-Jones J. Load-dependent kinetics of force production by smooth muscle myosin measured with optical tweezers. Nat Cell Biol. 2003; 5:980–986. [PubMed: 14578909]
34. Howard, J. Mechanics of Motor Proteins and the Cytoskeleton. Sinauer; Sunderland, Massachusetts: 2001. p. 229-244.
35. Clemen AEM, et al. Force-dependent stepping kinetics of myosin-V. Biophys J. 2005; 88:4402–4410. [PubMed: 15764664]
36. Syed S, Snyder GE, Franzini-Armstrong C, Selvin PR, Goldman YE. Adaptability of myosin V studied by simultaneous detection of position and orientation. EMBO J. 2006; 25:1795–1803. [PubMed: 16601691]
37. Forgacs E, et al. Kinetics of ADP dissociation from the trail and lead heads of actomyosin V following the power stroke. J Biol Chem. 2008; 283:766–773. [PubMed: 17965414]
38. Hannemann DE, Cao WX, Olivares AO, Robblee JP, De La Cruz EM. Magnesium, ADP, and actin binding linkage of myosin V: Evidence for multiple myosin V-ADP and actomyosin V-ADP states. Biochemistry. 2005; 44:8826–8840. [PubMed: 15952789]
39. Vilfan A. Elastic lever-arm model for myosin V. Biophys J. 2005; 88:3792–3805. [PubMed: 15792977]
40. Nyitrai MG, MA. Adenosine diphosphate and strain sensitivity in myosin motors. Philos Trans R Soc Lond, Ser B: Biol Sci. 2004; 359:1867–77. [PubMed: 15647162]
41. Nishizaka T, Miyata H, Yoshikawa H, Ishiwata S, Kinosita K. Unbinding force of a single motor molecule of muscle measured using optical tweezers. Nature. 1995; 377:251–254. [PubMed: 7675112]

42. Duke TAJ. Molecular model of muscle contraction. Proc Natl Acad Sci USA. 1999; 96:2770–2775. [PubMed: 10077586]

43. Shimamoto Y, Suzuki M, Ishiwata S. Length-dependent activation and auto-oscillation in skeletal myofibrils at partial activation by Ca2+ Biochem Biophys Res Commun. 2008; 366:233–238. [PubMed: 18061572]

44. Hudspeth AJ, Gillespie PG. Pulling springs to tune transduction - adaptation by hair-cells. Neuron. 1994; 12:1–9. [PubMed: 8292354]

45. Kruse K, Julicher F. Oscillations in cell biology. Curr Opin Cell Biol. 2005; 17:20–26. [PubMed: 15661515]

46. van Mameren J, Vermeulen KC, Gittes F, Schmidt CF. Leveraging Single Protein Polymers To Measure Flexural Rigidity. J Phys Chem B. 2009; 113:3837–3844. [PubMed: 19673071]

47. Sakmann, B.; Neher, E. Single Channel Recording. Plenum Press; New York: 1995. Single Channel Recording; p. 558-563.

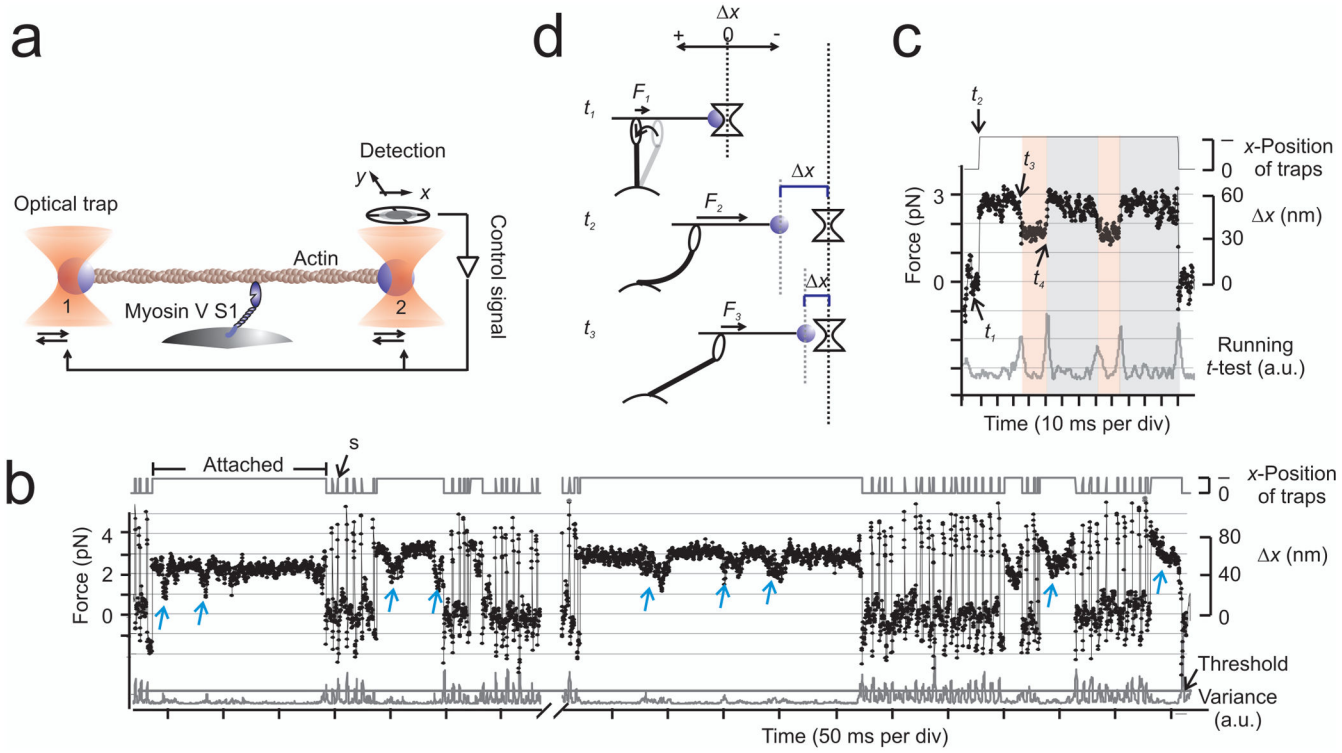

Figure 1.

Single MVS1 molecules interacting with actin under load**. (a)** MVS1 on surface attached beads interacting with F-actin suspended between two polystyrene beads held in optical traps. On-line detection of myosin binding was used to control trap position and to trigger trap displacement parallel to the actin filament axis to apply load. **(b)** Displacements produced by bound myosin at different resisting forces (5 kHz sampling rate). Δ*x* is bead position relative to trap position and determines force *F* on myosin; $F = 2\kappa_{trap}\Delta x$; κ_{trap}: single trap stiffness. The threshold to trigger trap displacement was tuned to keep the trap positions fixed during attached periods while spurious trap displacements (arrow *s*) were tolerated during unbound periods. **(c)** In a typical binding event initial binding and conformational change in +Δ*x* direction occurred around time point t_1 at ~ 0.5 pN load and were not resolved separately. Load was applied at time t_2 and at t_3 a negative displacement (see also blue arrows in Fig 1b) occurred, consistent with power stroke reversal, followed by a positive displacement at t_4. **(d)** Cartoon shows the sequence of trap displacement and bead movement when force is applied. Significant back and forth displacements were detected using a running *t*-test. The experiments were carried out at 100 μM ATP.

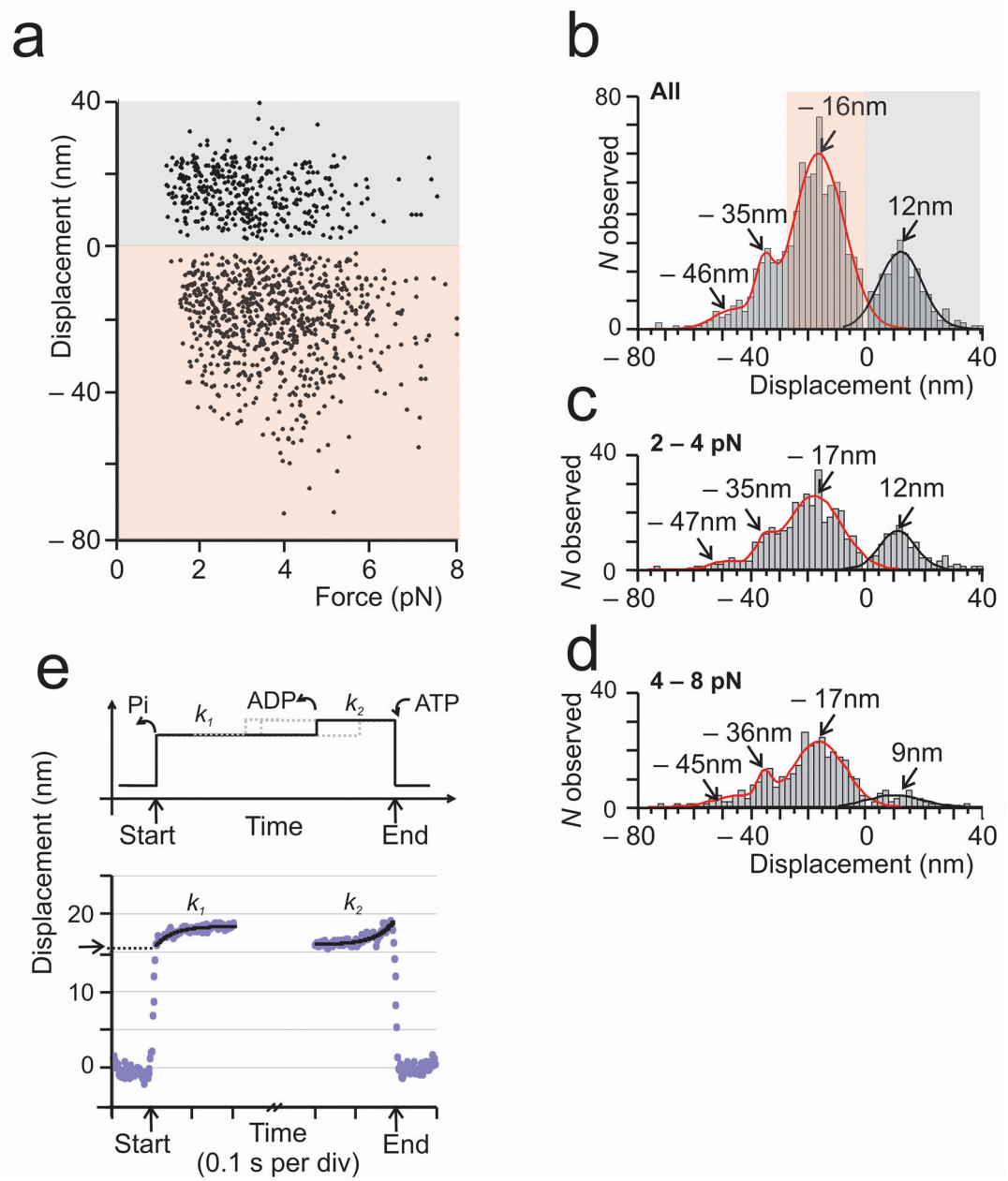

Figure 2.

Statistical analysis of reversals and recoveries. Negative displacements ('reversals') and positive displacements ('recoveries') were detected using a running *t*-test. **(a)** Amplitudes of reversals (red) and recoveries (grey) were measured relative to the level preceding the displacement step and plotted against load. **(b)** Distributions of reversals and recoveries (N= 1020), measured over 2 – 7 pN forces, were fitted by sums of Gaussians. **(c,d)** Subsets of reversals and recoveries were measured over 2 – 4 pN and 4 – 8 pN respectively. **(e)** Ensemble averaging [4] of binding events (N = 225) was used to determine amplitudes and transition rates of the MVS1 two-step power stroke at low load (< 2 pN) and low ATP (10 μM ATP). The model describes the two sub-steps of the MVS1 power stroke coupled to the

release of hydrolysis products phosphate and ADP. The dashed lines indicate stochastic timing of ADP release (k_1 = 24 s^{-1}). The nucleotide-free state following ADP release is terminated by ATP binding (k_2 = 23 s^{-1}) ref[6,7,26].

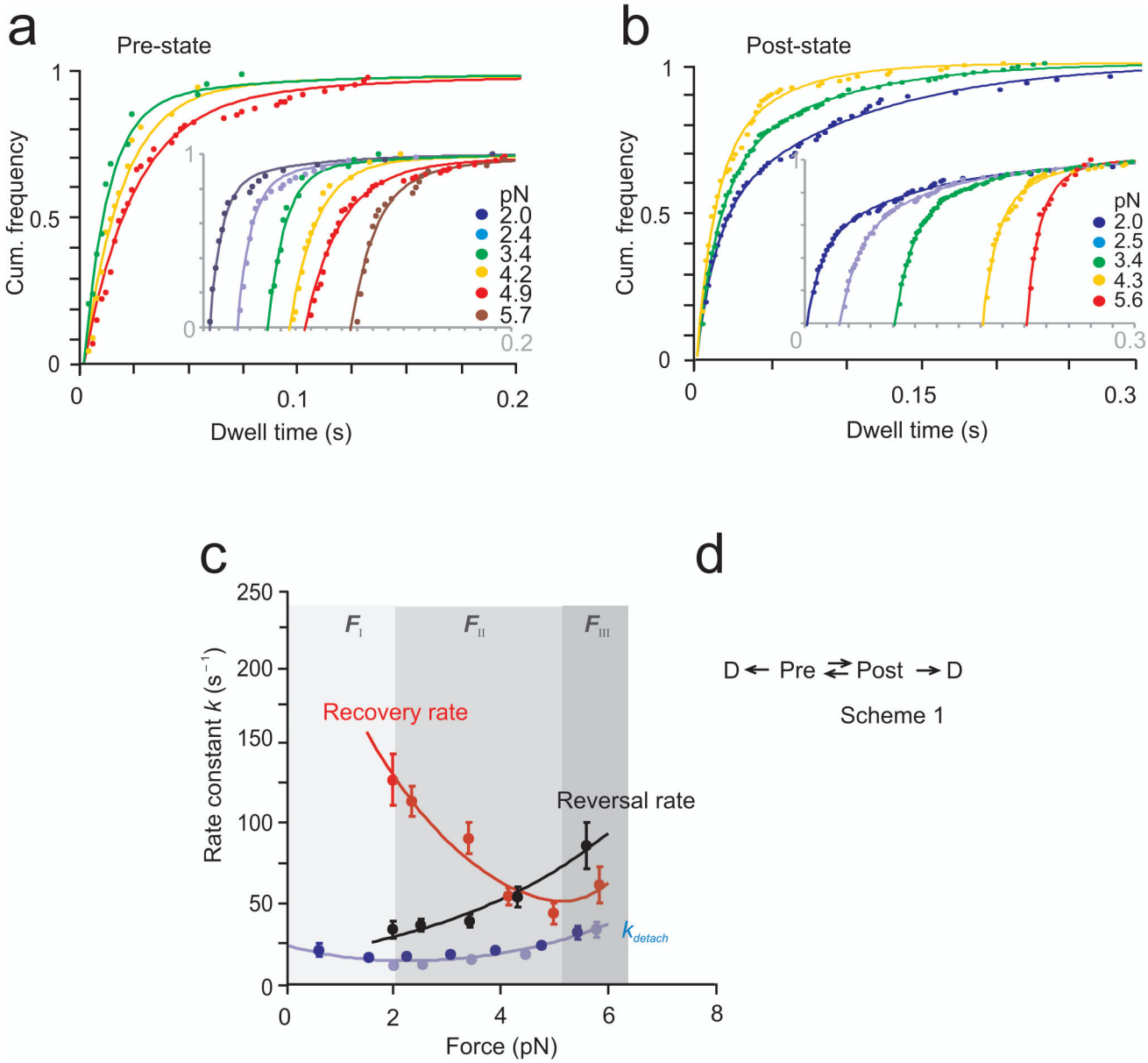

Figure 3.

Kinetics of pre and post-states. **(a)** Cumulative dwell-time distribution plots of the pre-state are described by a single exponential function and yield the recovery rate (eq. 1). **(b)** Two exponential components (eq. 2) were required to describe dwell times of the post-states and yield two reversal rates. Insets: plots at different loads were offset along the time axis for clarity. **(c)** Reversal and recovery rates are plotted against load. The two post-states in **(b)** (see Supplementary Fig. S2) were lumped into one and a single reversal rate was calculated (eq. 3). Load dependence of recovery rates was described by two exponential components (eq. 5), with k_{01} = 284 s $^{-1}$;d_1 = – 1.5 nm; k_{02} =0.03 s $^{-1}$; d_2 = 4.6 nm. Load dependence of reversals was described by a single exponential (eq. 4) with k_0 = 17 s $^{-1}$; d = 1.2 nm. The detachment rates, k_{detach} = (average time bound) $^{-1}$, are plotted versus load (see

Supplementary Fig. S2); k_{detach} for binding events with and without reversals are plotted in light and dark blue respectively (see Supplementary Fig. S4). Load dependence of the rates was described by two exponential components (eq. 5); k_{01} = 22 s $^{-1}$;d_1 = – 2.1 nm; k_{02} = 3.5 s $^{-1}$; d_2 = 1.6 nm. Experiments were carried out at 100 μM ATP. Rate constants and statistics are tabulated in Supplementary Table 1. F_{I}, F_{II} and F_{III} mark three force regimes for which no reversals (F_I)**,** reversals and recoveries (F_{II}) or forced detachments (F_{III}) were observed. **(d)** The model describes transitions between pre- and post-power stroke states and detachment (D).

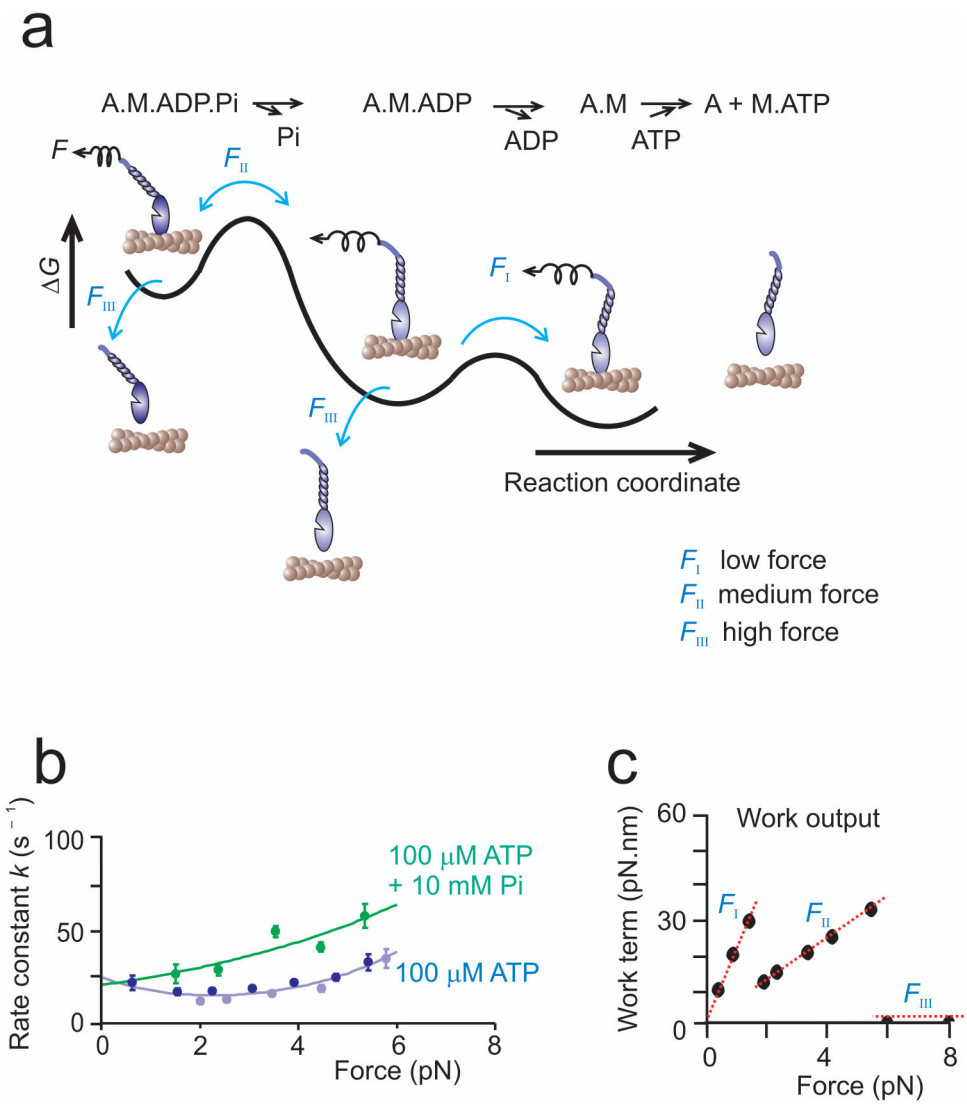

Figure 4.

Effect of load on a single myosin-V motor head. **(a)** The model summarises the effect of low (F_I)**,** medium (F_{II})**,** and high loads (F_{III}) on the chemo-mechanical cycle of a single myosin-Va motor head. **(b)** Rate constants characterising the average dwell time of MVS1 bound to actin in absence and presence of 10 mM phosphate are plotted versus load. Load dependence in presence of 10 mM phosphate was described by a single exponential function (eq. 4), with $k_{(0)}$ = 24 s^{-1} and d = 0.6 nm (see also Supplementary Fig. S4c). For comparison load dependence of dwell times in absence of added phosphate are plotted in blue (data from Fig. 3c). **(c)** Efficiency of energy conversion of a single motor head in the three load regimes (F_I – F_{III}).